In Vivo Mapping of Microstructural Somatotopies in the Human Corticospinal Pathways

Timothy Verstynen, Kevin Jarbo, Sudhir Pathak and Walter Schneider

J Neurophysiol 105:336-346, 2011. First published 10 November 2010;
doi: 10.1152/jn.00698.2010

Journal of Neurophysiology publishes original articles on the function of the nervous system. It is published 12 times a year (monthly) by the American Physiological Society, 9650 Rockville Pike, Bethesda MD 20814-3991.
 ISSN: 0022-3077, ESSN: 1522-1598. Visit our website at http://www.the-aps.org/.

J Neurophysiol 105: 336–346, 2011.
First published November 10, 2010; doi:10.1152/jn.00698.2010.

In Vivo Mapping of Microstructural Somatotopies in the Human Corticospinal Pathways

Timothy Verstynen,[1,2] Kevin Jarbo,[1] Sudhir Pathak,[1,2] and Walter Schneider[1,2,3]
[1]*Learning Research and Development Center,* [2]*Center for the Neural Basis of Cognition, and* [3]*Department of Psychology; University of Pittsburgh, Pittsburgh, Pennsylvania*

Submitted 6 August 2010; accepted in final form 10 November 2010

Verstynen T, Jarbo K, Pathak S, Schneider W. In vivo mapping of microstructural somatotopies in the human corticospinal pathways. *J Neurophysiol* 105: 336–346, 2011. First published November 10, 2010; doi:10.1152/jn.00698.2010. The human corticospinal pathway is organized in a body-centric (i.e., somatotopic) manner that begins in cortical cell bodies and is maintained in the axons as they project through the midbrain on their way to spinal motor neurons. The subcortical segment of this somatotopy has been described using histological methods on non-human primates but only coarsely validated from lesion studies in human patient populations. Using high definition fiber tracking (HDFT) techniques, we set out to provide the first in vivo quantitative description of the midbrain somatotopy of corticospinal fibers in humans. Multi-shell diffusion imaging and deterministic fiber tracking were used to map white matter bundles that originate in the neocortex, navigate complex fiber crossings, and project through the midbrain. These fiber bundles were segmented into premotor (dorsal premotor, ventral premotor, and supplementary motor area) and primary motor sections based on the cortical origin of each fiber streamline. With HDFT, we were able to reveal several unique corticospinal patterns, including the cortical origins of ventral premotor fibers and small (~1–2 mm) shifts in the midbrain location of premotor versus primary motor cortex fibers. More importantly, within the relatively small diameter of the pyramidal tracts (~5 mm), we were able to map and quantify the direction of the corticospinal somatotopy. These results show how an HDFT approach to white matter mapping provides the first in vivo, quantitative mapping of subcortical corticospinal topographies at resolutions previously only available with postmortem histological techniques.

INTRODUCTION

The corticospinal pathway consists of long axon bundles that project directly from cortical areas to motor neurons in the spine (Vulliemoz et al. 2005). While integral for the direct control of muscles, only half of these fibers originate in the primary motor cortex (M1) with the rest distributed across various higher-level motor planning areas (see Fig. 1*A*) (Dum and Strick 1991, 2005). Electrophysiological work (Godschalk and Mitz 1995; Penfield and Boldrey 1937) has established that most of these precentral motor regions exhibit a body-centric topography, i.e., somatotopy (dashed arrows in Fig. 1*A*) (see Geyer et al. 2000a for review). For example, in the motor areas along the central sulcus and precentral gyrus (M1 and the dorsal premotor cortex; PMd), lower extremity muscles are represented dorsally while upper extremity muscles are distributed in an anterior-lateral direction along the central sulcus. In contrast, for cells in the supplementary motor area (SMA), this lower-to-upper body spectrum occurs in a purely anterior direction (i.e., upper body cells are anterior to lower body cells).

Early lesion studies in rats and non-human primates showed that these cortical somatotopies are maintained in the descending projections that pass through the internal capsule and the midbrain (Barnard and Woolsey 1956). In the cerebral peduncle, fibers are organized such that axons projecting to lower body muscles are represented in lateral segments of the pyramidal tract, while fibers projecting to upper body muscles are represented in more medial segments (see Fig. 1*B*). In humans, this somatotopy within the peduncle has only been coarsely confirmed in rare focal lesion patients (Bucy et al. 1964; Leestma and Noronha 1976; Warabi et al. 1987). The relatively small spatial extent of the pyramidal tract within midbrain (~5 mm diam) has limited attempts to map this somatotopy using conventional structural or functional imaging methods.

Diffusion imaging methods, such as diffusion tensor imaging (DTI), have had some success at mapping the human corticospinal pathways. Fiber tracking algorithms applied to DTI data have successfully segregated the major segments of the midbrain tracts: i.e., frontopontine, mediopontine, and parietotemporopontine sections (Habas and Cabanis 2007; Lazar and Alexander 2005; Stieltjes et al. 2001). Even within these major segments there has been some success at differentiating premotor from primary motor fibers (Newton et al. 2006). However, the standard tensor model used by DTI has some limitations that prevent it from capturing more subtle micostructural characteristics of the motor system. In particular, the DTI model has been shown to have a limited capability in navigating complex fiber crossings (see Wedeen et al. 2005). This is particularly problematic when studying the topography of corticospinal fibers because it limits the ability of DTI to map more lateral aspects of the corticospinal tract, such as projections to ventral premotor cortex (PMv) and upper body regions of M1 (Tomassini et al. 2007). Given the direction of somatotopy in M1 and PMd, this can severely limit any attempt to characterize the topography of these pathways as they project to the spine. However, recent advances in high angular resolution imaging methods, such as diffusion spectrum imaging (DSI), have shown significant promise in overcoming the fiber crossing problem (Granziera et al. 2009; Hagmann et al. 2006; Wedeen et al. 2005, 2008).

Here we set out to provide the first in vivo mapping of the subcortical somatotopy of corticospinal fibers in humans. This necessitates imaging techniques that can track fibers from cortex, through complex fiber crossings, to subcortical targets with at least millimeter resolution. We utilize the term high

Address for reprint requests and other correspondence: T. Verstynen, Learning Research and Development Center, University of Pittsburgh, 3939 O'Hara St., Room 631, Pittsburgh, PA 15260 (E-mail: timothyv@pitt.edu).

definition fiber tracking (HDFT) to describe techniques that meet this criteria. Here we combine high directional DSI (Wedeen et al. 2008) with generalized Q-sampling imaging (GQI) and orientation diffusion function (ODF) filtered deterministic tractography (Yeh et al. 2010) to produce HDFT of the corticospinal fibers. This type of diffusion based tractography provides sufficient resolution to confirm several projection patterns previously only identified in the non-human primate. More importantly, with this information we are able to provide a statistically based method for quantifying corticospinal somatotopies in vivo.

METHODS

Participants

Five neurologically healthy adults (4 male; all right handed; age range: 22–31) from the local University of Pittsburgh community took part in this experiment, conducted as part of a larger data collection effort associated with the 2009 Pittsburgh Brain Competition. All participants were prescreened prior to scanning to rule out any contraindications to MR imaging. The procedures used here were all approved by the internal review board at the University of Pittsburgh and written consent was obtained from all participants prior to testing.

Image acquisition and reconstruction

DSI data were acquired on 3T Tim Trio System (Siemens) using a 32-channel coil. This involved a 43-min, 257-direction scan using a twice-refocused spin-echo EPI sequence and multiple q values (TR = 9,916 ms, TE = 157 ms, voxel size = 2.4 × 2.4 × 2.4 mm, FoV = 231 × 231 mm, b-max = 7,000 s/mm^2). For anatomical comparisons, we also included high resolution anatomical imaging, employing a 9-min T1-weighted axial MPRAGE sequence (TR = 2,110 ms, TE = 2.63 ms, flip angle = 8°, 176 slices, FoV = 256 × 256 mm^2, voxel size = 0.5 × 0.5 × 1.0 mm^3). DSI data were reconstructed using a GQI approach (Yeh et al. 2010). The ODFs were reconstructed to 362 discrete sampling directions and a mean diffusion distance of 1.2.

Fiber tracking and analysis

For the HDFT datasets, all fiber tracking was performed using DSIStudio (http://dsi-studio.labsolver.org). Rather than adopt a whole brain fiber tracking procedure, we chose to use an ODF-streamlined ROI based approach (Yeh et al. 2010). This was done to maximize the number of corticospinal projections detected and ignore irrelevant fiber pathways. For each hemisphere, a region of interest (ROI) mask was drawn on a single axial midbrain slice, covering the lateral wings of the cerebral peduncle (illustrated in Fig. 1*B*). A second ROI mask was drawn over the voxels with principle diffusion directions in the ventral-dorsal direction on the most ventrally acquired slice. In all subjects, the lowest acquired slice was too dorsal to guarantee isolation of only spinal projections (i.e., before the point of pyramidal decussation). Thus this second mask allowed avoidance of major cerebellar projections, i.e., the cerebellar peduncles, which also pass through the midbrain. A third ROI mask was drawn to cover all ipsilateral cortical areas to the cerebral peduncle ROI. This served as a seed region for the fiber-tracking algorithm. Finally, all voxels in the contralateral hemisphere were masked to create a region of avoidance (ROA) area for the fiber tracking algorithm. Fiber streamlines that extended to this region were excluded from the final dataset.

Once the ROIs were drawn, we tracked fibers by seeding any point in the third ROI mask until 175,000 streamlines were obtained that met the search criteria, i.e., streamlines that originated anywhere in ipsilateral cortex, continued through any point of the peduncle and continued past the point of cerebellar pathway divergence. The number of tracked fibers was set to a constant value to maintain approximately equal fiber densities across subjects. The specific value of 175,000 streamlines reflects the maximum number of corticospinal fibers that can be tracked in all subjects based on software constraints (e.g., before memory failures with the analysis program).[1] Tracks were generated using an ODF-streamline version of the FACT algorithm (Basser et al. 2000; Lazar et al. 2003; Yeh et al. 2010). Using a random seeding approach, we initiated tracking, from each random position within the seed mask (see preceding text), in the direction of the most prominent fiber. Fiber progression continued with a step size of 0.5 mm, minimum fiber length of 20 mm, and turning angle threshold of <70°. To smooth each track, the next directional estimate of each voxel was weighted by 20% of the previous moving direction and 80% by the incoming direction of the fiber. The tracking was terminated when the relative FA for the incoming direction dropped below a preset threshold (0.03–0.06 depending on the subject) or exceeded a turning angle of 70°. The FA termination threshold was adjusted on a per subject basis depending on the relative signal to noise of each scan, to maximize fiber projections to more lateral motor areas. Once tracked, all streamlines were saved in the TrackVis file format.

Cortical ROI selection

For each subject and each hemisphere, anatomically defined ROI masks were drawn on the subject's FA map to isolate cortical motor areas in DSI space. Four ROIs were drawn on each hemisphere to cover the precentral agranular cortex (Fig. 1A). ROIs were labeled to correspond with their predominant macroscopic structural landmarks: caudal and rostral precentral gyrus (cPCG and rPCG), dorsomedial PCG and superior frontal gyrus (dmPCG-SFG), and ventral PCG and inferior frontal gyrus (vPCG-IFG). The anatomical locations of each ROI mask were segmented to approximate neuroanatomical locations of cortical motor areas (see Geyer et al. 2000a for review). All ROIs were drawn on the axial slices, selected primarily gray matter, and followed the anatomical constraints defined as follows:

cPCG. Voxels along the anterior wall of the central sulcus were selected starting at the deepest boundary of the sulcus (where M1 and somatosensory cortex meet) and drawn along the sulcus and up on to the caudal aspects of the PCG, approximately the posterior third of the gyrus. Drawing started with the most dorsal visible aspects of the central sulcus and continued ventrally on a slice-by-slice basis until the tip of the ascending ramus of the inferior frontal gyrus was visible. Voxels in this mask are drawn so as to completely encompass M1 and portions of PMd.

rPCG. The caudal border of this mask began on the voxel immediately adjacent to the most anterior cPCG voxel. Voxels were selected from this point, along the medial and anterior aspects of the PCG, and down the posterior aspect of the precentral sulcus. Drawing started just below the level of the dmPCG-SFG mask (see next) extending ventrally to the same slice as cPCG. Voxels in this mask are drawn so as to cover the anterior aspects of PMd.

dmPCG-SFG. The caudal border of this mask abutted the anterior voxels of the dorsal part of the cPCG mask. Voxels were drawn to cover the most superior and medial portions of the precentral and superior frontal gyri. Drawing began on the most superior visible slice and continued ventrally until the level of the superior frontal sulcus was visible. The most rostral border of this mask ended at the point of the pre-SMA dimple. This mask is drawn to encompass all of SMA.

vPCG-IFG. Voxels for this mask were selected beginning at the most ventral border of the rPCG and cPCG masks. Gray matter

[1] Of course the theoretical upper-bound of the number of tracked tracked fibers is the number of underlying fiber bundles present in each corticospinal pathway.

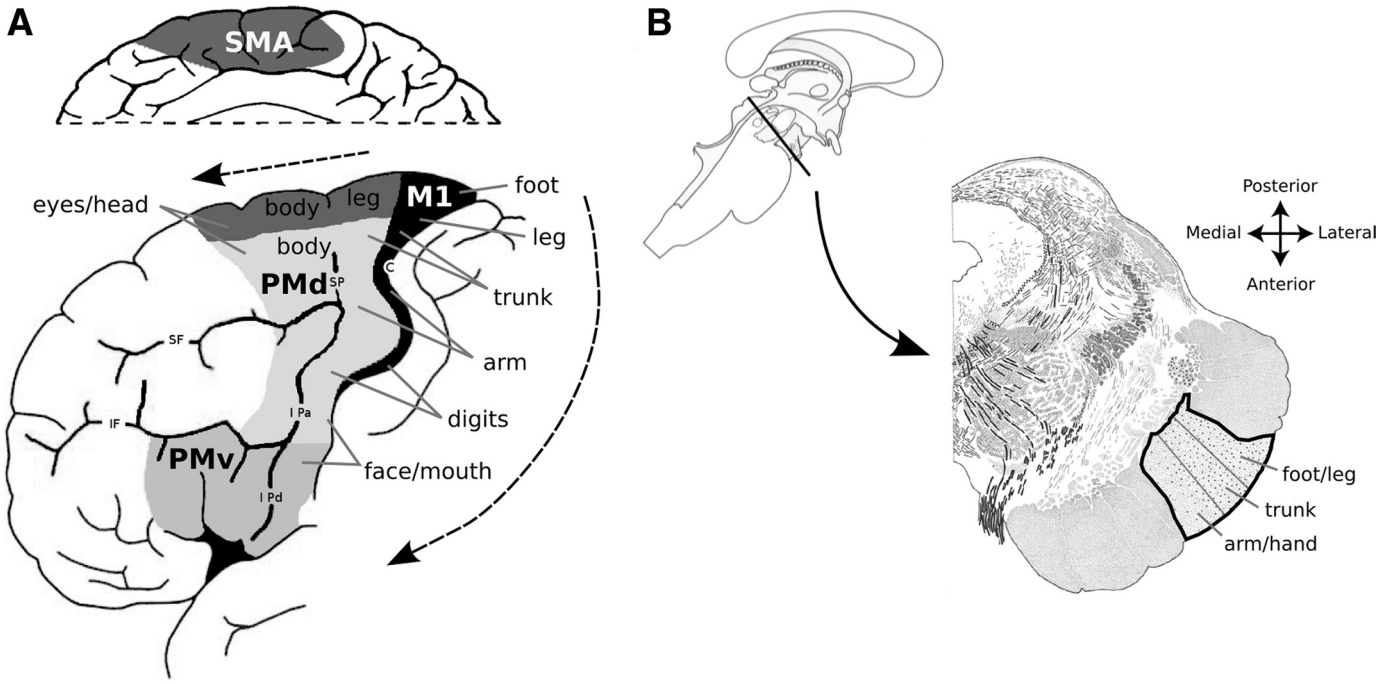

FIG. 1. *A*: the spatial organization of precentral lateral motor areas. All areas in gray and black reflect the precentral distribution of the agranular cortex. Within these regions there exist 2 directions of somatotopy (dashed arrows). The first is expressed in a lateral-anterior-ventral direction along the precentral gyrus and central sulcus, reflecting a shift from lower- to upper-body muscles. The second, found in supplementary motor area (SMA), is expressed in a purely anterior direction. Modified from Rizzolatti et al. 1998 (via Geyers et al. 2000a). See text for further details (C, central sulcus; IF, inferior frontal sulcus; SF, superior frontal sulcus; Ipa, inferior precentral sulcus ascending aspect; Ipd, inferior precentral sulcus descending aspect; SP, superior precentral sulcus). *B*: cutout of the left cerebral peduncle. The pyramidal section of the midbrain fibers, that contains the corticospinal pathways, is outlined.

voxels in the entire PCG, precentral sulcus and the inferior frontal gyrus were selected. Drawing was terminated at the point of the Sylvian Fissure. This mask is drawn so as to contain voxels thought to be in PMv.

Figure 2 shows the average ROI mask for all five subjects projected into MNI template space (see following text) as well as the intersection mask for voxels consistently marked in at least three subjects to illustrate the minimal overlap of identified voxels on the single subject level. The different subsections of the corticospinal tract were then categorized by isolating the fiber streamlines that intersected with each cortical ROI. These tracts were saved as separate files for subsequent analysis (see following text).

Pilot work had shown that our methods could not detect projections from cingulate medial wall areas known to have direct corticospinal projections in nonhuman primates. Therefore these areas were excluded from analysis.

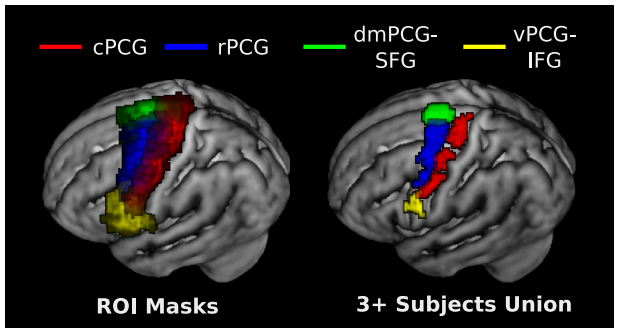

FIG. 2. The region of interest (ROI) masks averaged across all subjects. Left: the overlay of all masks for all 5 participants. Right: voxels in each mask that are consistently present for at least 3 participants.

Data analysis

AVERAGED FIBER DENSITY AND ROI MASKS. For display purposes, fiber density maps and ROI masks were transformed into MNI space, while microstructural analysis was performed in the individual subject DSI space (see following text). Density maps show the number of fibers present in each voxel. These maps were generated for each ROI in TrackVis (www.trackvis.org) by selecting only those fibers that intersect with the targeted ROI mask and saving output image maps reflecting the density of fibers in each voxel. The output density map was in the same space as the subject's DSI image. To perform the MNI normalization, the transformation matrix from each subject's generalized FA (gFA) volume to a template gFA space was estimated using nonlinear registration method in SPM8 (ICBM space template regularization, 16 nonlinear iteration). The gFA is the degree of water anisotropy present in each voxel and is generally used as a map of overall white matter density. This normalization was then applied to the density maps and ROI masks for each subject using a trilinear interpolation method (1 mm^3 voxels). Once in MNI space, density maps and ROI masks were averaged across subjects.

STREAMLINE DISTRIBUTION ANALYSIS. All analysis of midbrain projection distributions from different primary and premotor regions was performed separately per hemisphere on fiber streamlines in individual subject's DSI space. A mid-brain mask was drawn for each subject on the same slice as used in the fiber tracking process (see preceding text). For each streamline, we recorded two coordinate values. First, we recorded the two-dimensional (2D) axial-plane coordinate values (i.e., x and y positions) as the streamline intersected with the midbrain ROI mask. Second, we recorded the 3D coordinate value (i.e., x, y, and z positions) of the streamline's origin in the neocortex. Because the fiber streamlines are dimensionless lines, all coordinate positions are recorded in subvoxel, millimeter values.

Two types of analysis were performed on these streamlines. First, we analyzed the fiber distribution pattern for streamlines originating in separate motor areas within each hemisphere. For this analysis, we normalized each 2D midbrain coordinate to the average x and y position of the cPCG fiber cluster of each subject. Directional shifts for the other regions were then recorded as a difference from the cPCG cluster. For display purposes, we calculated a density distribution for each ROI cluster using a 2D interpolation method (*interp2* in Matlab). These density distributions were then averaged across subjects.

Second, we quantified the integrity of the corticospinal somatotopy through the midbrain using a multivariate regression technique to see how a fiber's cortical position predicted its midbrain position. From neuroanatomy studies, we expect an anterior-medial shift in midbrain position as fibers move from lower-body to upper-body representations (Fig. 1*B*). For M1 and PMd fibers in both the cPCG and rPCG masks, we used a principle component analysis to identify the primary direction of the spatial distribution of fiber endpoints along the central sulcus and PCG (i.e., the anterior-lateral-ventral shift illustrated in Fig. 1*A*). An individual fiber's loading on the first principle component was then used as an estimate of its position along the direction of somatotopy with low values reflecting lower body areas and higher values reflecting upper body areas. For SMA fibers in the dmPCG-SFG mask, the cortical position along the sagittal plane (i.e., *y* position) was used as an index of its position along the direction of somatotopy. These index values for *N* fibers in each ROI were then *z*-score normalized for each subject and used as a $1 \times N$ regressor, Z_{soma}, to predict the 2D fiber position in the midbrain, Y_{pos}., represented by a $2 \times N$ vector. Values of Z_{soma} that were outside the 95% confidence level (i.e., >1.96 or less than -1.96) were set to the nearest confidence interval bound. This was done using the multivariate ordinary least squares regression model

$$Y_{pos} = \beta * Z_{soma} + \mu$$

The coefficent matrix, β, is a 2×1 matrix reflecting the shift in midbrain *x* and *y* positions as a fiber's cortical endpoint moves along the direction of somatotopy (i.e., $\beta = [\Delta_x \ \Delta_y]'$). The angle of this shift, in degrees, can then be computed from these values as

$$\theta_{shift} = 180/\pi * \arctan(\Delta_x/\Delta_y)$$

To account for slight differences in head angle of each subject, these shifts were normalized by rotating the shift angles according to the lateral plane of the cerebral peduncle (Fig. 3*A*).

To calculate the within-subject significance of the observed somatotopic shift, we devised a permutation statistic for circular data (Manly 1997). We opted for this approach over the more traditional Rayleigh test (Fisher 1995) because we wanted a statistical measure that takes both vector direction and vector magnitude into account. The logic of this statistic is that if the observed θ_{shift} was simply a random observation, then repeated scrambling of the input, i.e., Z_{soma}, and reestimating θ_{shift} should produce a uniform distribution of angles. However, if there is real underlying structure in the data, then the distribution of permuted values should deviate from a uniform distribution. Specifically, there should be a higher likelihood of observing angles near the observed direction, as well as in the opposite, i.e., 180° shifted, direction.

To illustrate this, we simulated a $2 \times N$ vector of hypothetical midbrain positions, $Y^*_{pos,}$ according to the model

$$Y^*_{pos} = \beta * Z^*_{soma} + N(0, \sigma)$$

where Z^*_{soma} is a uniformly selected set of simulated somatotopy points and $n = 4{,}000$. The shift strength (Δ) represents the degree of anisotropy in the simulated distribution, Y^*_{pos}, such that $\beta = [\Delta \ 2*\Delta]'$. In one simulation, Δ was set to 0 [i.e., $Y^*_{pos} = N(0,\sigma)$]. In another, Δ was set to 1 to produce a distribution with true underlying structure. For each simulated dataset, we first estimated the observed shift angle, $\theta_{observed,}$ as described in the preceding text. Next we permuted the model by randomly scrambling the values in Z^*_{soma} and re-estimated the new observed angle. This process was repeated for 4,000 iterations to generate a distribution of simulated values. The resulting distribution of simulated and observed angles is shown in Fig. 3*B*. As expected, the simulated data with real underlying structure (i.e., high anisotropy; $\Delta = 1$), exhibited two peaks about the observed angle and 180° away. In contrast, the dataset with no real structure (i.e., no anisotropy; $\Delta = 0$) appeared to have a purely uniform distribution.

To calculate the statistical significance of this deviation from the uniform distribution, we estimated the probability of observing a value within ± 9° of the nonpermuted value $\theta_{observed.}$ This was done by calculating the percentage of permuted values that fell within this range (dashed vertical lines in Fig. 3B*)*. Uniformly distributed data should, on average, should result in a cumulative probability near 5.28%. Highly structured data, in contrast, should have a higher probability. To see the full effect, we simulated a range of datasets with different of shift values and noise components (σ). Each simulated dataset underwent 100 permutation tests to estimate a 95% confidence interval (error bars in Fig. 3*C*). As expected, modeled

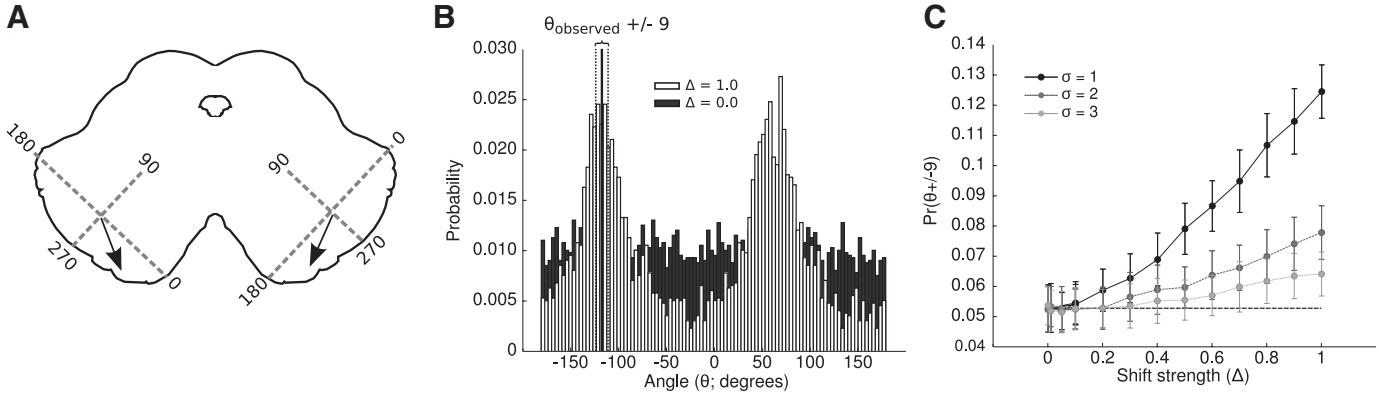

FIG. 3. *A*: example of the coordinate space used to display the somatotopic shift angles (see METHODS). The → shows hypothetical shift patterns in each hemisphere. *B*: example probability distributions from 2 simulated systems. The 1st system ($\Delta = 1$; □) has a high degree of structure relating a cortical position to a mid-brain position. The 2nd system ($\Delta = 0$; ▨) has no real underlying structure. The latter distribution is uniform when tested with a permutation test. The former distribution, with underlying structure, has 2 peaks at the simulated direction and 180° away. To estimate how far this distribution is from a uniform function, we took the cumulative distribution at the observed angle ($\theta_{observed}$; —) and ± 9° (- - -). *C*: the cumulative distribution within this target range is plotted as a function of the true underlying shift (Δ) and the noise in the model (σ; see METHODS). The — shows the chance levels expected by a uniform distribution. Error bars show the 95% confidence interval after 100 simulations. Simulations where this interval does not overlap with chance are considered statistically significant.

datasets with higher shift values quickly moved away from chance levels (horizontal dashed line). This effect was tempered in datasets with more underlying noise.

This same process (4,000 iteration permutation test with 100 repetitions to produce a 95% confidence interval, cumulative density between ± 9° of the observed value, etc) was applied to the observed data from each ROI mask. Fiber tracts whose lower bound exceeded the expected chance level of 5.28% probability were considered statistically significant.

RESULTS

Regional distributions of corticospinal projections

The motor area ROIs were anatomically localized based on the structural anatomy visible in each subject's generalized FA map. The borders between regions are approximate given that the true boundaries between these regions, in each subject, can only be definitively determined histologically (see Geyer et al. 2000a). To confirm that these maps encompass the appropriate functional areas, we looked at the percent overlap of each ROI with probabilistic maps of local Brodmann's areas (Table 1) (Amunts et al. 1999; Geyer 2004; Geyer et al. 1999, 2000a,b). As expected, the cPCG ROI encompassed both BA4 and BA6 regions with minimal overlap of sensory areas (BA1-3) and BA4 encompassing on average 27% of the ROI across both hemispheres. rPCG and dmPCG-SFG masks almost exclusively encompassed BA6, while the vPCG-IFG mask encompassed nonmotor areas BA44 and BA45. Since the identification of Broca's area (BA44 and BA45) as being "premotor" is currently under debate (Chouinard and Paus 2006; Kalplan and Iacoboni 2007; Tomassini et al. 2007; Wise 2006), it should be pointed out that a substantial portion (~40%) of the vPCG-IFG mask encompasses noncategorizable regions of the ventral PCG/sulcus (see following text). We discuss this in more detail below.

Consistent with previous tractography (Lazar and Alexander 2005; Newton et al. 2006) and monkey lesion studies (Levin 1936), we were able to detect a segregation of fibers from different cortical motor areas within the midbrain. The average fiber densities from each ROI are shown in Fig. 4 (see METHODS for fiber selection criterion). Although areas such as the ventral aspects of the rPCG and cPCG ROIs, as well as the vPCG-IFG mask, showed reduced fiber densities than more dorsal and medial areas, we were able to aggregate fibers from all cortical ROIs. We observed some degree of overlap between M1 and PMd regions encompassed in the cPCG and rPCG masks. This overlap is not surprising given that, as mentioned in the preceding text, there is not a clear macroscopic anatomical distinction to differentiate these two regions (Geyer et al. 2000a) and the normalization process can result in some blurring of these boundary areas when displayed on the template image (Diedrichsen 2006). Finally, the ventral premotor fibers in the vPCG-IFG mask tended to segregate exclusively in the anterior aspects of the PCG, consistent with previous imaging results of the position of the ventral premotor cortex (Chouinard and Paus 2006; Kalplan and Iacoboni 2007; Tomasssini et al. 2007).

Previous virus tracing studies of the corticospinal pathways in non-human primates have found that half of the corticospinal projections originate from neurons in M1 (Dum and Strick 1991, 2005). We found a similar pattern in the relative density of fiber streamlines (Fig. 5). Within each hemisphere, a majority of fibers originated in the cPCG mask, while the rPCG and dmPCG-SFT ROIs contain the next highest percentages. Overall the fewest fibers were found to originate in the vPCG-IFG ROI. This dominance of presumably M1 fibers in the cPCG mask was true in both the left [repeated measures $F(3,12) = 11.85$, $P < 0.0001$] and right [repeated measures $F(3,12) = 28.03$, $P < 0.0001$] hemisphere regions. Thus the relative distribution of fibers across areas generally matches neuroanatomical expectations.

Within the cerebral peduncle, the pyramidal tract resides in a medial section, encompassing ~1/3 of the total peduncular area (see Fig. 1*B*). The midbrain location of fiber streamlines originating from lateral motor areas matches this neuroantomical expectation (Fig. 6*A*). Nearly all fibers penetrated through the medial section of the peduncle. In addition, these projections tend to hug the lateral wall of the midbrain, suggesting that a majority of the tracked fibers reflect pyramidal tract axons rather than reticulospinal and cerebellar projections that generally project behind the pyramidals, in more medial and dorsal aspects of the midbrain (Nathan et al. 1990).

Previous diffusion imaging (Lazar and Alexander 2005; Newton et al. 2006; Stieltjes et al. 2001) and lesion (Levin 1936) studies have reported a segregation of midbrain projections depending on the cortical origin of the fibers (e.g., M1, PMd, SMA, etc). We were also able to observe a regional separation of the location of midbrain fibers that originate from different cortical motor areas. Figure 6*B* shows the fiber density distributions for each ROI, averaged across each subject's nonnormalized tractography space (see METHODS). In both hemispheres, the premotor regions were shifted ~1–2 mm in an anterior-medial direction from the cluster of fiber projec-

TABLE 1. *Percent ROI overlap with probabilistic cytoarchitectonic atlas*

	BA44 %	BA45 %	BA4a %	BA4p %	BA1 %	BA2 %	BA3a %	BA3b %	BA6 %
Left cPCG	6 ± 0.8	0 ± 0.1	24 ± 1.9	14 ± 1.3	0 ± 0.0	0 ± 0.0	4 ± 0.9	2 ± 0.3	44 ± 3.7
Left rPCG	9 ± 1.3	0 ± 0.2	1 ± 0.4	0 ± 0.1	0 ± 0.0	0 ± 0.0	0 ± 0.0	0 ± 0.0	27 ± 2.9
Left vPCG-IFG	50 ± 4.1	10 ± 2.6	0 ± 0.0	0 ± 0.0	0 ± 0.0	0 ± 0.0	0 ± 0.1	0 ± 0.0	0 ± 0.0
Left dmPCG-SFG	0 ± 0.0	0 ± 0.0	7 ± 2.9	0 ± 0.0	0 ± 0.0	0 ± 0.0	0 ± 0.0	0 ± 0.0	83 ± 4.8
Right cPCG	6 ± 1.2	0 ± 0.0	11 ± 1.1	5 ± 0.9	0 ± 0.0	0 ± 0.0	2 ± 0.2	1 ± 0.3	54 ± 2.7
Right rPCG	4 ± 1.1	0 ± 0.0	0 ± 0.3	0 ± 0.0	0 ± 0.0	0 ± 0.0	0 ± 0.0	0 ± 0.0	29 ± 4.2
Right vPCG-IFG	47 ± 5.7	17 ± 1.1	0 ± 0.0	0 ± 0.0	0 ± 0.0	0 ± 0.0	0 ± 0.0	0 ± 0.0	0 ± 0.0
Right dmPCG-SFG	0 ± 0.0	0 ± 0.0	4 ± 1.7	0 ± 0.0	0 ± 0.0	0 ± 0.0	0 ± 0.0	0 ± 0.0	84 ± 3.7

ROI, region of interest; cPCG and rPCG, caudal and rostral precentral gyrus; vPCG-IFG, ventral PCG and inferior frontal gyrus; dmPCG-SFG, dorsomedial PCG and superior frontral gyrus.

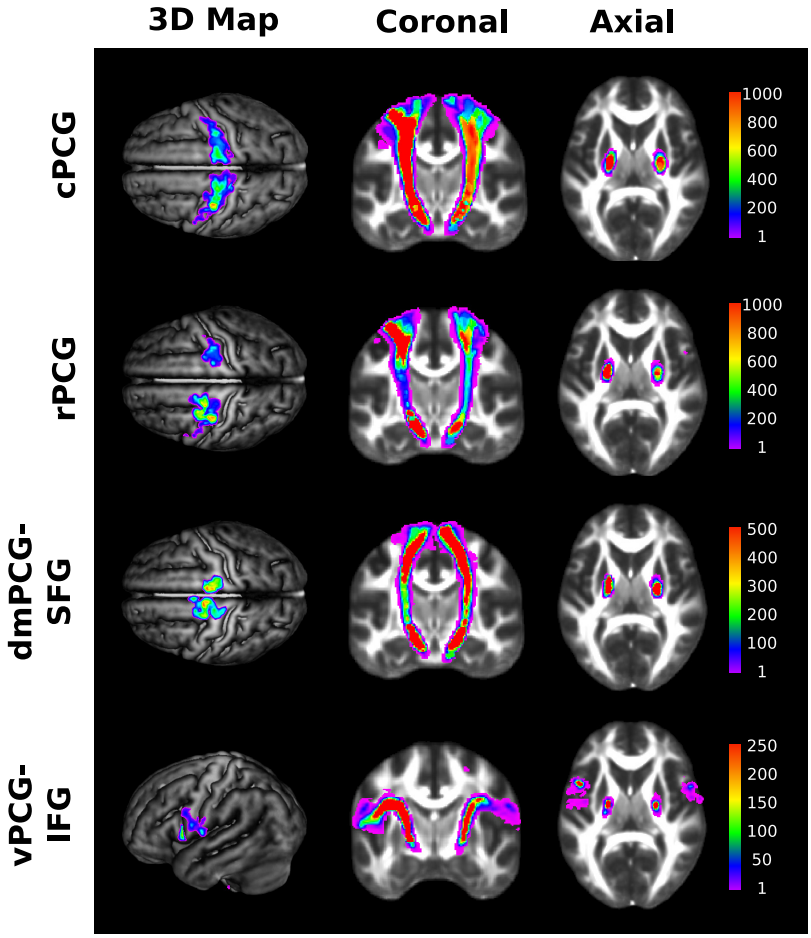

FIG. 4. Average fiber distribution patterns from each cortical ROI, projected onto the MNI generalized FA (GFA) template. Axial plane shows the fibers at the level of the internal capsule.

tions from the cPCG mask that contained the M1 fibers (all 1-sample *t*s >2.89, all *P*s <0.022).

Quantifying the somatotopy of corticospinal projections

Histological studies of non-human animals have shown that the fibers from cortical motor areas should converge and organize into a consistent somatotopic pattern (see Fig. 1*B*) (Barnard and Woolsey 1956). To detect this organization, we relied on the established cortical somatotopic patterns of the precentral motor areas. As is shown in Fig. 1*A*, the cortical motor areas have at least two linear somatotopies. A lower-to-upper extremity somatotopy in an anterior-lateral-ventral direction along the PCG and a lower-to-upper extremity somatotopy in an anterior direction in SMA (see Geyer et al. 2000a for review). When these projections penetrate through the cerebral peduncle, the effector representations converge along a single direction with fibers projecting to lower-body muscles located in lateral areas of the pyramidal tract and fibers projecting to upper-body muscles located in medial sections (see Fig. 1*B*).

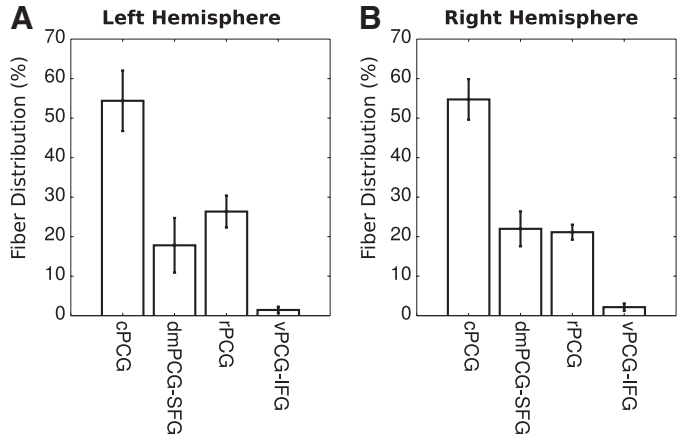

FIG. 5. *A*: average percentage of fibers terminating in each cortical ROI for the left hemisphere. Error bars show SE across subjects. *B*: same as *A* for right hemisphere projections.

Within our fiber tracks, we looked at how a fiber's cortical origin, along the plane of somatotopy, predicts the spatial location of its projection through the midbrain. Fibers from the vPCG-IFG ROI were excluded from this analysis because the direction of somatotopy in the ventral premotor cortex is not well understood. For M1 and PMd fibers in both the cPCG and rPCG masks, we categorized each streamline according to its position along the dominant direction of the central sulcus and PCG (see METHODS), with smaller values (red dots) reflecting lower-body regions of the somatotopy and larger values (blue dots) reflecting upper-body regions. Figure 7 shows a set of fibers originating in the cPCG ROI for an example subject. Consistent with lesion studies in nonhuman primates (Barnard and Woolsey 1956), lower-body fibers originating in the dorsal/medial areas of the central sulcus and PCG (*top inset*) were clustered in posterior and lateral sections of the peduncle (*bottom inset*). In

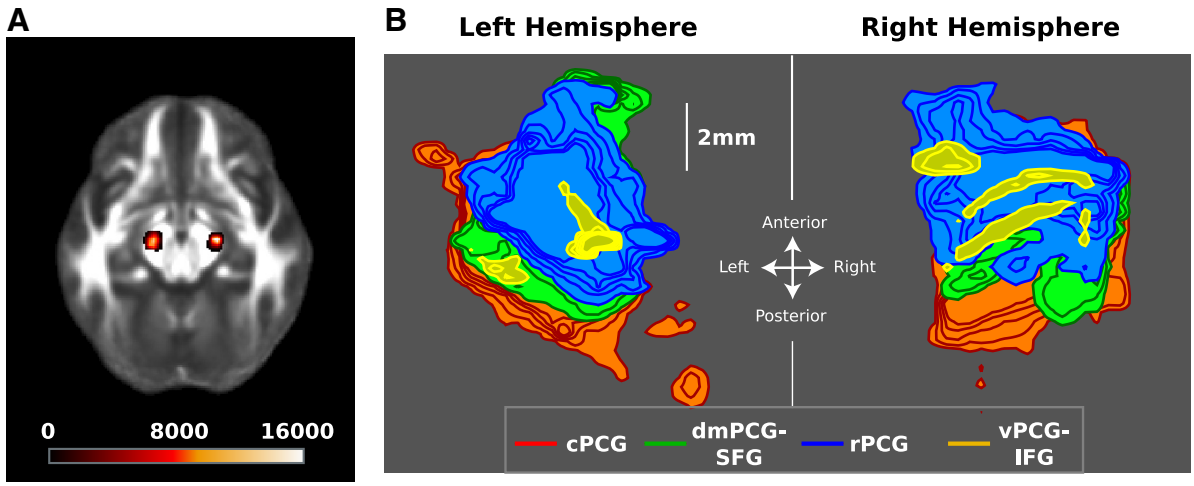

FIG. 6. *A*: average area of midbrain penetration for all fibers (collapsed across cortical ROI), at the level of the start of the cerebral peduncle. *B*: topographic maps showing the average distribution pattern from each cortical ROI in nonnormalized tractography space. Each concentric ring represents an increase in density of 25 fibers (peak threshold at 100+ fibers). The premotor clusters tended to be shifted 1–2 mm away from the center of the caudal precentral gyrus (cPCG) cluster.

contrast, upper-body fibers originating in more ventral-lateral aspects of the central sulcus and PCG were predominately observed in the anterior and medial aspects of the peduncle. Thus moving ventrally along the central sulcus and PCG resulted in a fiber's midbrain position being shifted in a medial and anterior direction.

If the midbrain projection pattern of M1 and PMd fibers in the cPCG mask is simply an artifact of the fiber tracking process, then we should not observe a similar lower-to-upper body projection pattern in SMA fibers. For example, if the fiber streamline arrangement reflects the erroneous mapping based simply on the predominant downward ODF orientations (e.g., fiber streamlines simply descend ventrally based on their starting location in cortex), then moving along the anterior direction of somatotopy in the SMA (see Fig. 1*A*) will simply result in an anterior shift of the fiber positions in the midbrain. However, as is shown in Fig. 8, we found that fibers originating in posterior aspects of the dmPCG-SFG mask, consistent with lower-body projections, clustered in posterior-lateral aspects of the peduncle. In contrast, fibers originating in anterior aspects of the dmPCG-SFG mask (i.e., upper-body projections) clustered in anterior-medial aspects of the peduncle.

To quantify this somatotopic shift, we used multivariate regression to model the position of midbrain fibers as their cortical origin moves from lower- to upper-body regions (see METHODS). We adopted a modified bootstrap procedure, for circular data, to assess the significance of each observed somatotopic shift on the individual-subject level. Figure 9*A* shows the relationship between an ROIs shift amplitude (i.e., how far moving along the cortical somatotopy caused a fiber to move across the midbrain) and the significance of that shift for all subjects and ROIs (chance level shown as vertical gray line;

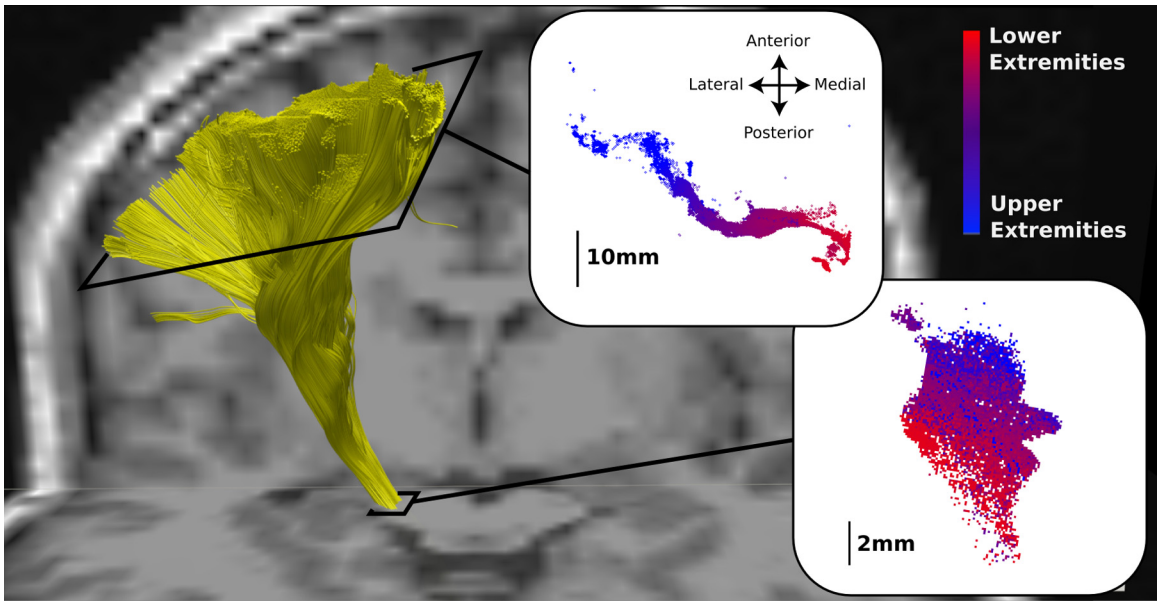

FIG. 7. Tracked primary motor cortex (M1) and dorsal premotor cortex (PMd) fibers that terminate in the cPCG ROI for a single subject are shown in yellow (75% of the total fibers are shown). *Top inset*: the distribution of the cortical endpoints, viewed in the axial plane, as they project down the somatotopy of the central sulcus and PCG. *Bottom inset*: the same fibers as they penetrate the midbrain, also in the axial plane.

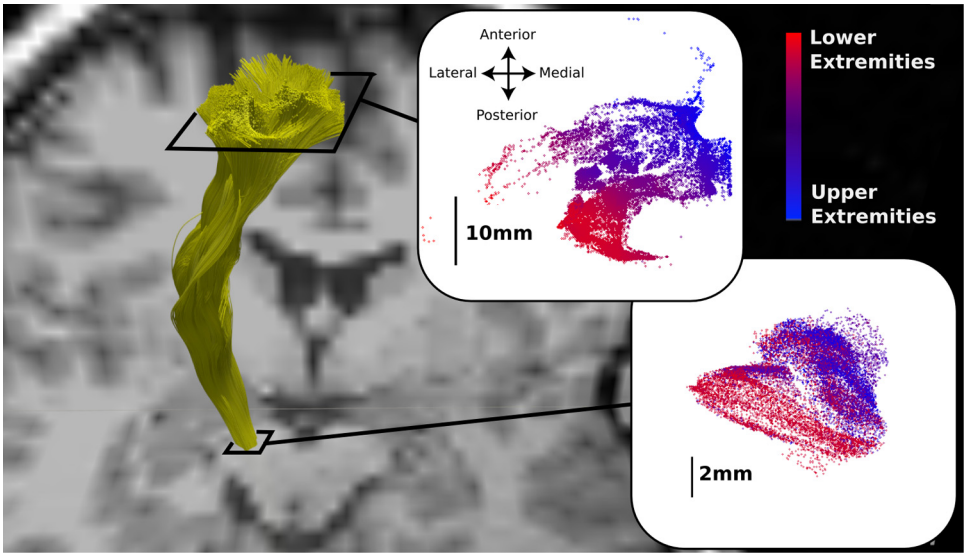

FIG. 8. Tracked SMA fibers that originate in the dorsomedial PCG and superior frontal gyrus (dmPCG-SFG) ROI for a different subject than shown in Fig. 7 (75% of the total fibers are shown). *Top inset*: the distribution of the cortical endpoints as they project anteriorly across the SMA somatotopy. *Bottom inset*: the same fibers as they penetrate the midbrain. Otherwise the same viewing conventions as Fig. 7.

see METHODS). Across all regions and subjects, fiber projections with larger shift amplitudes tended to be statistically significant (black circles in Fig. 9*A*) at the individual subject level, while smaller shift amplitudes tended to not be significant (gray circles; $R^2 = 0.47$, slope = 32.32, $P < 0.001$). This correlation fits with the predictions from simulated datasets (Fig. 3*C*). The average shift amplitude was 2.45, which means that moving 1 SD along the direction of somatotopy in cortex shifts a fiber's position in the midbrain ~2.5 mm.

When looking at the direction of these somatotopic shifts we found that for fibers originating from the cPCG masks, there was a consistent anterior-medial shift across all subjects in both

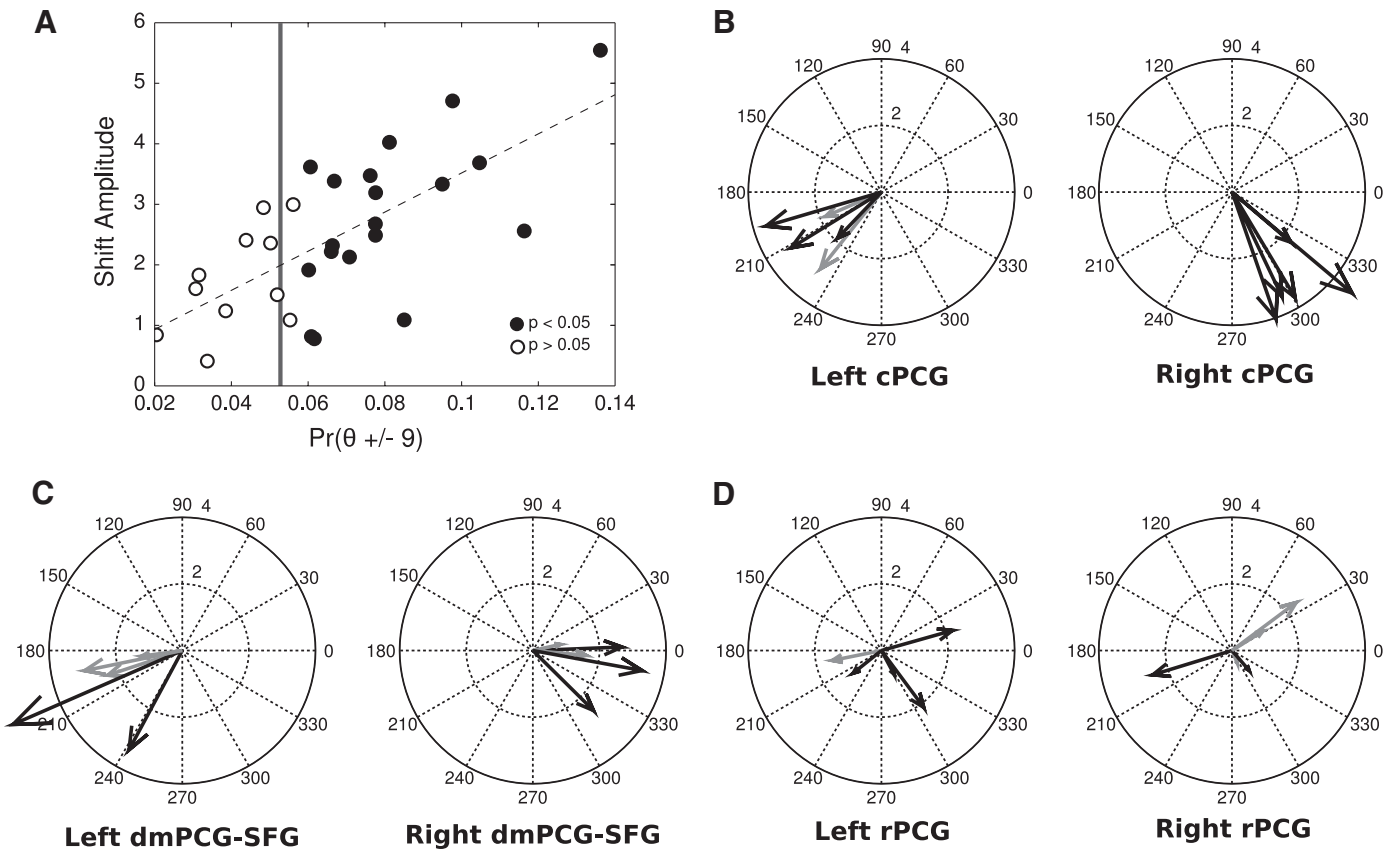

FIG. 9. *A*: the relationship between somatotopic shift amplitude and the cumulative distribution about the observed shift direction according to a permutation statistic (see METHODS). Data reflect shifts for fibers in the caudal PCG (cPCG), rostral PCG (rPCG) and dorsomedial PCG and superior frontal gyrus (dmPCG-SFG) ROIs. White circles, nonsignificant shifts and black circles reflect statistically significant shifts; vertical gray line, the expected permutation statistic from chance; dashed line, the regression line for the relationship. *B*: each arrow represents the angle and amplitude of somatotopic shift from cPCG fibers for individual subjects. Figure 3*A* illustrates the coordinate frames for each hemisphere. Black arrows show significant shifts while gray arrows show nonsignificant shifts. *C*: same as *B* for dmPCG-SFG. *D*: same as *B* for rPCG.

hemispheres (Fig. 9*B*). In most cases, this shift was statistically significant at the individual subject level (black arrows; only 2 P values >0.05), particularly for projections from the right hemisphere where this was significant for every subject. Between hemispheres the mean shift direction was oriented in a predominantly medial and anterior direction (mean left vector = 213°, mean right angle = 305°; see Fig. 3*A* for reference frame). To see whether the vector shift was significant at the group level, we used a Rayleigh test (Fisher 1995). This showed significant clustering in both the left ($P = 0.0028$) and right hemisphere ($P = 0.0027$). The robustness of this shift at the single-subject level and its consistency across subjects (left hemisphere $\text{range}_{|\min\theta\text{-}\max\theta|}$ = 24°, right hemisphere $\text{range}_{|\min\theta\text{-}\max\theta|}$ = 39°) provides further validation on the reliability of the HDFT approach in mapping the corticospinal pathways.

In addition to M1 and PMd fibers in the cPCG mask, we also observed similar distributions of somatotopic shift angles for SMA projections originating in the dmPCG-SFG mask (Fig. 9*C*). Moving in an anterior direction, i.e., from lower- to upper-body representations, resulted in medial midbrain shifts across subjects. This effect was noisier at the single subject level than the cPCG fibers, with significant shifts detected in 6 of 10 ROIs. However, all subjects expressed similar projection directions across both hemispheres (left hemisphere $\text{range}_{|\min\theta\text{-}\max\theta|}$ = 42°, right hemisphere $\text{range}_{|\min\theta\text{-}\max\theta|}$ = 29°). These vector shifts were clustered in a more medial direction than those from the cPCG mask but still significant at the group level in both the left (mean vector = 204°, $P = 0.0047$) and right hemisphere (mean vector = 351°, $P = 0.0047$).

Finally, we were unable to detect an anterior-medial shift pattern in the rPCG ROI mask (Fig. 9*D*). However, this is not surprising given that the somatotopy of this area of PMd is less linearly distributed (Aflalo and Graziano 2006). Not surprisingly, the Rayleigh's test did not reveal a significant clustering of vectors (both Ps > 0.38). We discuss the lack of quantified somatotopy in these fibers in more detail in the following text.

DISCUSSION

We have shown how combining multi-shell diffusion imaging, GQI reconstruction and deterministic fiber tracking can provide subvoxel/submillimeter resolution of fiber topographies in the human corticospinal pathway. This HDFT approach allowed for the first in vivo validation of the midbrain coticospinal somatotopies that were previously only mapped in nonhuman species. Our analysis showed that fibers originating in cortical areas that represent lower body muscles tended to project through lateral aspects of the pyramidal tract in the cerebral peduncle. As a fiber's origin moves to more upper-body representations, the location of its midbrain projection moves medially. This effect was observed from fibers originating in two distinct cortical areas with different somatotopic patterns. More importantly, the direction of this midbrain organization is consistent histological studies in rats and nonhuman primates (Barnard and Woolsey 1956).

While we were able to confirm the somatotopic shift from fibers in the cPCG and dPCG-SFG ROIs, we did not see a consistent organizational pattern in fibers originating from the rostral precentral ROI. Part of this may be due to the fact that the cPCG mask encompasses both M1 and PMd fibers. Distinguishing M1 from PMd fibers is presently impossible with MRI due to the inability to isolate their shared boundary using visible anatomical landmarks. It is this caudal aspect of the PMd that contains the somatotopies that descend along the PCG just as their M1 counterparts (see Fig. 1*A*). The topographic organization of more rostral premotor aspects of the PCG contain less linearly arranged representations (Affalo and Graziano 2006) making it difficult to capture the midbrain somatotopies with the methods used in this paper. Future work may elucidate this by refining the anatomical masks used to delineate M1 and PMd on the single subject level (Geyer 2004; Geyer et al. 2000a,b). In addition, it may be possible to use a fiber's midbrain position to predict its somatotopic representation. In this way the more complex representational structure of both PMd and PMv fibers (see next paragraph) can be mapped based on the subcortical fiber positions. This is also left up to future work.

Another particularly interesting observation is the origin of ventral premotor corticospinal projections in the vPCG-IFG mask (Fig. 4). These fibers originated primarily in the PCG and *not* in more frontal agranular cortex regions (see also Wise 2006). The location of these projections is consistent with functional magnetic resonance imaging observations showing that PMv is situated between BA44 and BA3 regions, along the border of the PCG and inferior frontal junction (Chouinard and Paus 2006; Kalplan and Iacoboni 2007; Tomasssini et al. 2007). Thus while the agranular cortex in humans may encompass higher, nonpremotor cytoarchitectonic regions, the descending projections from ventral areas originate from a relatively concentrated area of cortex.

The ability to obtain the resolution needed to map these subcortical pathways with HDFT stems from two key factors. First, the combination of multishell high angular resolution imaging (Wedeen et al. 2005, 2008) with a modified GQI reconstruction method (Yeh et al. 2010) allows for a more efficient reconstruction of the resulting ODFs. This combination of established methods provided sufficient directional information to allow deterministic fiber tracking algorithms to navigate areas with multiple fiber crossings. This fiber crossing problem is a limitation with the standard tensor model in other diffusion imaging techniques such as DTI (see Wedeen et al. 2005, 2008). In the corticospinal pathway, navigating fiber crossings is particularly important since projections to lateral and ventral motor areas intersect with the fibers of the arcuate fasciculus and corpus callosum (Nathan et al. 1990). While we still found a higher density of fibers in medial and dorsal motor areas, we were able to get sufficient coverage to ventral motor areas to detect somatotopic shifts along the PCG, as well as identify fibers projecting to ventral premotor cortex.

Second, by applying a focal ROI based tracking, we were able to acquire a sufficiently large enough sample of corticospinal projections to observe fiber somatotopies in the midbrain. Typical tractography methods tend to focus on mapping the entire brain and then subselecting relevant fiber streamlines of interest (Granziera et al. 2009; Habas and Cabanis 2007; Wedeen et al. 2008). By focusing on tracking only a specific pathway, i.e., the corticospinal fibers, we were able to produce a relatively high density of fiber streamlines (see also Lazar

and Alexander 2005; Newton et al. 2006). This provided sufficient statistical power needed to detect and quantify the microscopic structure in our target pathway. Indeed pilot work in our lab using other diffusion imaging (e.g., q-ball reconstructed HARDI and standard DSI reconstruction models, etc) and fiber tracking methods (i.e., whole brain FACT tracking) was unable to detect either somatotopic structure or regional segregation of fibers through the midbrain.

While our HDFT approach did allow for a sufficient resolution to detect subcortical fiber topographies, there are still several ways in which we were unable to detect key characteristics of the motor pathway. For example, while we did get sufficient coverage of fibers below the hand notch of the central sulcus, there was still a bias toward tracking fibers in more medial and dorsal aspects of lateral motor areas. This reflects a persistent inefficiency in navigating fiber crossings. This spatial bias in tracking may also be the reason why the relative fiber densities to PMd and PMv that we observed do not match the predictions from non-human primate studies (Dum and Strick 1991, 2005). In addition, this may explain why we were unable to detect corticospinal projections from medial wall cingulate areas that are known to exist in the nonhuman primate (Dum and Strick 1996).

Regardless of these technical limitations, we were able to successfully validate that the topography of axons in the human pyramidal tract follow similar projection patterns as mapped in non-human primates: i.e., medial-lateral somatotopy, segregation of primary motor and premotor cortex fibers, etc. This mapping of corticospinal topography in the midbrain is impossible with the current spatial resolution of standard T1 weighted images (~0.5–1 mm maximum resolution). This presents a lower bound of spatial resolution that is well above the level of individual axon clusters. It is also impossible to functionally image these pathways with functional brain imaging techniques. For example, fMRI only measures metabolic changes at the level of the dendrites and cell bodies, not along the axons (Logothetis et al. 2001). The HDFT methods that we employed provide both the ability and resolution with which to explore these connections. Along with validating patterns found in the non-human primate, these mapping techniques can also be used to identify novel structural topographies that may be uniquely human. Of course, such novel patterns can only be confirmed through direct histological validation as well.

The in vivo nature and single-subject sensitivity of this mapping technique may eventually be able to provide a utility for clinical mapping of white matter pathways. For example, given the density of fiber projections in the midbrain, even relatively small lesions can introduce profound behavioral impairments (Bucy et al. 1964; Leestma and Noronha 1976). Precision at identifying the fibers that are lesioned can optimize diagnostic methods for assessing motor pathologies (Stinear et al. 2007) and provide better monitoring of physiological changes in the recovery process. Of course, this can be applied outside of the motor system to identify diffuse axonal injury from a variety of etiologies (Maller et al. 2010). Finally, this kind of mapping can optimize the presurgical planning process, to reduce the damage to eloquent fibers during resections of subcortical pathologies (Fernandez-Miranda et al. 2010).

ACKNOWLEDGMENTS

The authors thank J. Phillips and P. Strick for helpful comments on the early stages of his project. This work was supported by DARPA contract NBCHC070104.

DISCLOSURES

No conflicts of interest, financial or otherwise, are declared by the author(s).

REFERENCES

Aflalo T, Graziano M. Possible origins of the complex topographic organization of motor cortex: reduction of a multidimensional space onto a two-dimensional array. *J Neurosci* 26: 6288–6297, 2006.

Amunts K, Schleicher A, Burgel U, Mohlberg H, Uylings HB, Zilles K. Broca's region revisited: cytoarchitecture and intersubject variability. *Brain* 412: 319–341, 1999.

Barnard J, Woolsey C. A study of localization in the corticospinal tracts of monkey and rat. *J Comp Neurol* 105: 25–50, 1956.

Basser P, Pajevic S, Pierpaoli C, Duda J, Aldroubi A. In vivo fiber tractography using DT-MRI data. *Magn Reson Med* 44: 625–632, 2000.

Bucy P, Keplinger J, Siqueira E. Destruction of the "pyramidal tract" in man. *J Neurosurg* 21: 385–397, 1964.

Chouinard PA, Paus T. The primary and premotor areas of human cerebral cortex. *Neuroscientist* 12: 143–152, 2006.

Diedrichsen J. A spatially unbiased atlas template of the human cerebellum. *NeuroImage* 33: 127–138, 2006.

Dum RP, Strick PL. The origin of corticospinal projections from the premotor areas in the frontal lobe. *J Neurosci* 11: 667–669, 1991.

Dum RP, Strick PL. Frontal lobe inputs to the digit representations of the motor areas on the lateral surface of the hemisphere. *J Neurosci* 25: 1375–1386, 2005.

Fernandez-Miranda J, Engh J, Pathak S, Madhok R, Boada F, Schneider W, Kassan A. High-definition fiber tracking guidance for intraparenchymal endoscopic port surgery. *J Neurosurg* 113: 990–999, 2010.

Fisher NI. *Statistical Analysis of Circular Data.* Cambridge, UK: Cambridge Univ. Press, 1995.

Geyer S. The microstructural border between the motor and the cognitive domain in the human cerebral cortex. *Adv Anat Embryol Cell Biol* 174: 1–89, 2004.

Geyer S, Matelli M, Luppino G, Zilles K. Functional neuroanatomy of the primate isocortical motor system. *Anat Embryol* 202: 443–474, 2000a.

Geyer S, Schleicher A, Zilles K. Areas 3a, 3b, and 1 of human primary somatosensory cortex. *NeuroImage* 10: 63–83, 1999.

Geyer S, Schormann T, Mohlberg H, Zilles K. Areas 3a, 3b, and 1 of human primary somatosensory cortex. *NeuroImage* 11: 684–696, 2000b.

Godschalk M, Mitz AR. Somatotopy of monkey premotor cortex examined with microstimulation. *Neurosci Res* 23: 269–279, 1995.

Granziera C, Schmahmann JD, Hadjikhani N, Meyer H, Meuli R, Wedeen V, Krueger G. Diffusion spectrum imaging shows the structural basis of functional cerebellar circuits in the human cerebellum in vivo. *PloS One* 4: 1–6, 2009.

Habas C, Cabanis EA. Anatomical parcellation of the brainstem and cerebellar white matter: a preliminary probabilistic tractography study at 3 T. *Neuroradiology* 849–863, 2007.

Hagmann P, Jonasson L, Maeder P, Thiran J, Wedeen VJ, Meuli R. Understanding diffusion MR imaging techniques: from scalar diffusion-weighted imaging to diffusion tensor imaging and beyond. *Radiographics* 26: 205–224, 2006.

Kalplan J, Iacoboni M. Multimodal action representation in human left ventral premotor cortex. *Cogn Process* 8: 103–113, 2007.

Lazar M, Alexander AL. Bootstrap white matter tractography (BOOT-TRAC). *Measurement* 24: 524–532, 2005.

Lazar M, Weinstein DM, Tsuruda JS, Hasan KM, Arfanakis K, Meyerand ME, Badie B, Rowley HA, Haughton V, Field A, Alexander AL. White matter tractography using diffusion tensor deflection. *Hum Brain Mapp* 18: 306–321, 2003.

Leestma JE, Noronha A. Pure motor hemiplegia, medullary pyramid lesion, and olivary hypertrophy. *J Neurol, Neurosurg Psychiatry* 39: 877–884, 1976.

Levin P. The efferent fibers of the frontal lobe of the monkey (*Macaca mulatta*). *J Comp Neurol* 63: 369–419, 1936.

Logothetis NK, Pauls J, Augath M, Trinath T, Oeltermann A. Neurophysiological investigation of the basis of the fMRI signal. *Nature* 412: 150–157, 2001.

Maller JJ, Thomson RH, Lewis PM, Rose SE, Pannek K, Fitzgerald PB. Traumatic brain injury, major depression, and diffusion tensor imaging: making connections. *Brain Res Rev* 64: 213–240, 2010.

Manly B. *Randomization, Bootstrap and Monte Carlo Methods in Biology* **(2nd ed.)**. New York: Chapman and Hall, 1997.

Nathan P, Smith M, Deacon P. The corticospinal tracts in man: course and location of fibers at different segmental levels. *Brain* 113: 303–324, 1990.

Newton JM, Ward NS, Parker GJ, Deichmann R, Alexander DC, Friston KJ, Frackowiak RSJ. Non-invasive mapping of corticofugal fibres from multiple motor areas—relevance to stroke recovery. *Brain* 1844–1858, 2006.

Penfield W, Boldrey E. Somatotopic motor and sensory representation in the cerebral cortex of man as studied by electrical stimulation. *Brain* 60: 389–443, 1937.

Stieltjes B, Kaufmann WE, Fredericksen K, Pearlson GD, Solaiyappan M, Mori S. Diffusion tensor imaging and axonal tracking in the human brain stem. *NeuroImage* 735: 723–735, 2001.

Stinear CM, Barber PA, Smale PR, Coxon JP, Fleming MK, Byblow WD. Functional potential in chronic stroke patients depends on corticospinal tract integrity. *Brain* 130: 170–180, 2007.

Tomassini V, Jbabdi S, Klein JC, Behrens TE, Pozzilli C, Matthews PM, Rushworth MFS, Johansen-Berg H. Diffusion-weighted imaging tractography-based parcellation of the human lateral premotor cortex identifies dorsal and ventral subregions with anatomical and functional specializations. *J Neurosci* 27: 10259–10269, 2007.

Vulliemoz S, Raineteau O, Jabaudon D. Reaching beyond the midline: why are human brains cross wired? *Rev Lit Arts Am* 4: 87–99, 2005.

Warabi T, Miyasaka K, Inoue K, Nakamura N. Computed tomographic studies of the basis pedunculi in chronic hemiplegic patients: topographic correlation between cerebral lesion and midbrain shrinkage. *Neuroradiology* 29: 409–415, 1987.

Wedeen VJ, Hagmann P, Tseng WY, Reese TG, Weisskoff RM. Mapping complex tissue architecture with diffusion spectrum magnetic resonance imaging. *Magn Reson Med* 54: 1377–86, 2005.

Wedeen J, Wang P, Schmahmann D, Benner T, Tseng I, Dai G, Pandya DN, Hagmann, P, D'Arceuil H, de Crespigny, A.J. Diffusion spectrum magnetic resonance imaging (DSI) tractography of crossing fibers. *NeuroImage* 41: 1267–1277, 2008.

Wise SP. The ventral premotor cortex, corticospinal region C, and the origin of primates. *Cortex* 42: 521–524, 2006.

Yeh F, Wedeen VJ, Tseng WI. Generalized q-sampling imaging. *IEEE Trans Med Imaging*, In Press.